

# 1. Introduction

Numerical simulations were conducted on synthetic digital rocks containing predefined non-ellipsoidal pore geometries. The objective was to determine the behavior of the perturbation coefficients  $a$  and  $b$  introduced in the Extended Differential Effective Medium (Ex-DEM) Theory (Paper Reference in Zenodo record description).

The document describes the construction of the pore models, their spatial distribution within the computational mesh, the simulation methodology, and the post-processing procedures applied to the resulting stress-strain data. A brief overview of the Ex-DEM formulation is provided to introduce the perturbation coefficients and their relationship with pore geometry.

The simulated effective bulk and shear moduli are then fitted to the Ex-DEM model to establish quantitative correlations between pore morphology – captured through parameters such as aspect ratio and convexity – and the perturbation coefficients. Finally, the results are presented for different pore families, highlighting how deviations from ideal ellipsoidal geometry influence the values of  $a$  and  $b$ .

# 2. OpenFOAM

OpenFOAM – Open Field Operations and Manipulation is an open-source computational fluid dynamics (CFD) and continuum mechanics solver that provides a flexible framework for solving partial differential equations using the finite-volume method. In this work, all numerical simulations were performed on foam-extend 4.1 on an Ubuntu 18.04 linux environment. The solver elasticSolidFoam was employed to compute the static elastic response of synthetic digital rocks containing pores with predefined geometry. This solver, based on finite-volume method, solves the equation of linear elasticity to obtain the displacement, strain, and stress fields within the solid domain under prescribed boundary conditions. The simulations were carried out under quasi-static loading, ensuring that

inertial effects were negligible. The stress-strain data obtained from these runs were used to calculate the effective bulk and shear moduli of each model, which were subsequently fitted to the Extended Differential Effective Medium (Ex-DEM) formulation to determine perturbation coefficients  $a$  and  $b$ .

### 3. Pore Models and Distribution

Two distinct families of synthetic pore geometries were generated to systematically examine the sensitivity of the Extended Differential Effective Medium (Ex-DEM) perturbation coefficients  $a$  and  $b$  to changes in pore shape and convexity. These simplified, idealized models isolate purely geometric effects, allowing direct comparison between different shape parameters without the influence of pore connectivity or mineral heterogeneity.

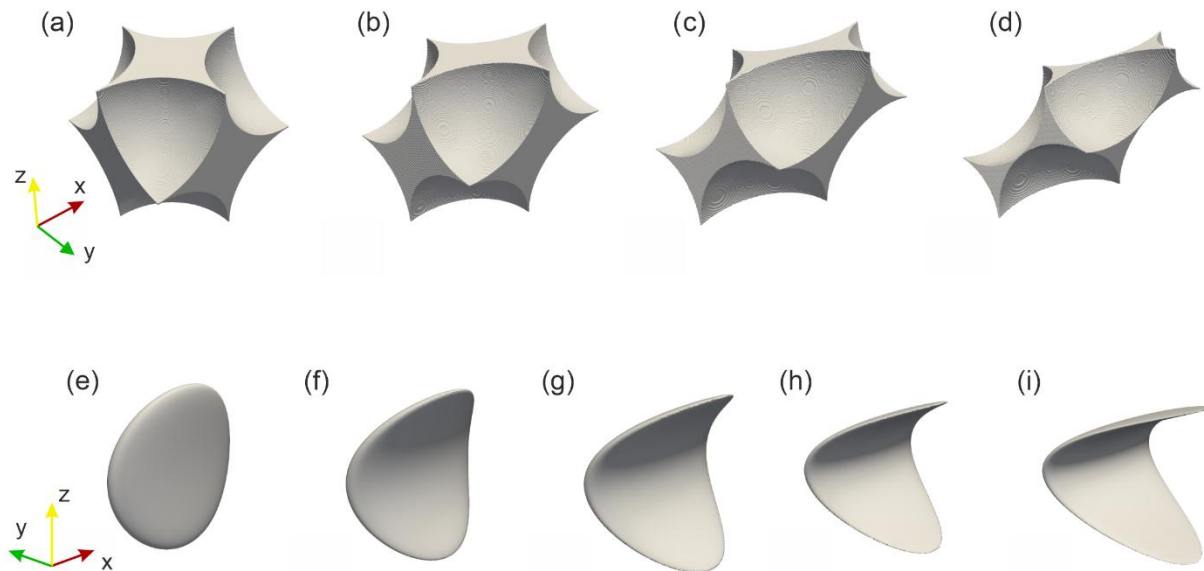


*Figure 1: Synthetic pore geometries used for numerical simulations to study the effects of pore shapes on extended DEM parameters. (a-d) Rhombohedral sphere-packing configuration showing variation in the inter-edge angle  $\chi = 90^\circ, 80^\circ, 70^\circ$ , and  $60^\circ$ . Decreasing  $\chi$  increases the skewness of the unit cell, producing progressively elongated pore shape with decreasing convexity. (e-i) Ellipsoidal models with controlled convexity,*

generated by applying a parabolic deformation parameter  $\delta = 0.2, 0.4, 1.0, 1.4$ , and  $1.8$  for a fixed  $r = 1$  and  $\alpha = [1.0, 0.25, 1.0]$ . Increasing  $\delta$  introduces concavity along the  $y$ -axis, resulting in a gradual loss of convexity relative to the reference ellipsoid.

### 3.1 Rhombohedral Sphere-Packing Configuration

The first family consists of rhombohedral shape-packing pores constructed within a unit cell defined by the three equal-length edge vectors meeting at a common inter-edge angle  $\chi$ .

By varying  $\chi$ , the unit cell transitions from cubic configuration ( $\chi = 90^\circ$ ) to increasingly skewed or elongated arrangements ( $60^\circ \leq \chi \leq 90^\circ$ ). Each pore is formed as the region enclosed by the rhombohedron but lying outside the union of eight identical spheres positioned at the cell vertices.

This geometric construction provides a controlled way to vary pore convexity while maintaining consistent pore size and symmetry (Zhouhui Lian et al., 2012). A decrease in  $\chi$  systematically reduces convexity, producing a family of shapes ranging from nearly spherical to strongly concave forms.

### 3.2 Ellipsoidal Model with Gradually Varying Convexity

The second pore family comprises ellipsoidal models whose shapes are modified using a parabolic deformation parameter,  $\delta$ .

Starting from the standard ellipsoidal equation,

$$\frac{x^2}{a_x^2} + \frac{y^2}{a_y^2} + \frac{z^2}{a_z^2} \leq 1$$

A parabolic term is added along the  $y$ -axis to introduce curvature asymmetry:

$$\frac{x^2}{a_x^2} + \frac{(y + \delta z^2)^2}{a_y^2} + \frac{z^2}{a_z^2} \leq 1$$

Here,  $\delta = 0$  corresponds to a perfect ellipsoid, while decreasing  $\delta$  introduces concavity along the deformation axis, producing a continuous transition from smooth convex pores to more complex, inward-curved geometries.

This parametric deformation allows direct control over convexity while maintaining a fixed overall aspect ratio, making it well suited for studying the geometric sensitivity of  $a$  and  $b$

### 3.3 Random Distribution Scheme

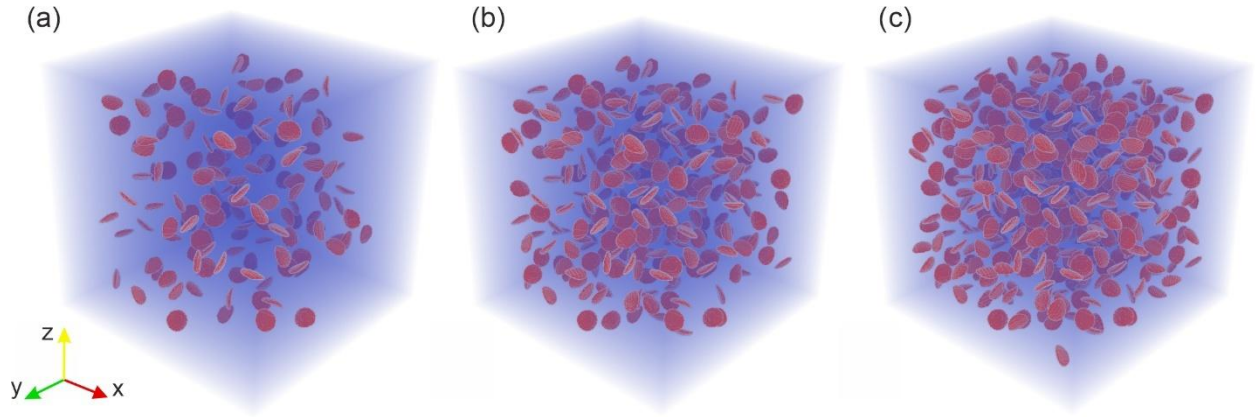


*Figure 2: Random distribution of ellipsoidal pores with  $\alpha = [1.0, 0.25, 1.0]$  and  $\delta = 0.2$  at porosities (a)  $\phi = 1\%$  (b)  $\phi = 2\%$  and (c)  $\phi = 3\%$ . The pores are spaced sufficiently apart to reduce the stress field interaction and are positioned away from boundary to mitigate boundary effects.*

To satisfy the dilute-inclusion assumption of the Differential Effective Medium (DEM) framework, pores were distributed randomly within a cubic computational domain using a custom placement algorithm designed to prevent overlapping and ensure statistical isotropy. Each pore shape – ellipsoidal or rhombohedral – was initially enlarged by a dilation factor, temporarily increasing its size to maintain adequate separation between neighboring inclusion during placement. The algorithm then searched for random positions and orientation of these enlarged pores within the cube while enforcing two constraints: (i) no overlap between any two pores, and (ii) fixed separation from the domain boundaries.

During iterative placement process, the porosity  $\phi$  of the mesh with original pore was continuously tracked. Once the desired porosity was reached the determination of acceptable positions and orientation is complete. The enlarged pores were replaced with their original-sized counterparts, preserving the random orientation and spacing. This approach ensures that pores remain non-interacting while maintaining a realistic, randomly oriented distribution throughout the sample. The inherent randomness of placement and orientation produces an effectively isotropic medium at the sample scale, while the controlled spacing preserves the validity of the DEM assumption.

## 4. Simulation Methodology

All simulations were performed using the “elasticSolidFoam” solver from foam-extend 4.1 running on Ubuntu 18.04. The workflow links a voxel-based pore geometry, generated from 3-D microstructural data, with OpenFOAM’s finite-volume elasticity framework through a custom-built mesh conversion algorithm.

### 4.1 Mesh Generation from 3-D images

Each model began with a binary 3-D image of size 350x350x350 voxels, representing the pore-solid microstructure, with voxels assigned to values of 1 (solid) and 0 (pore). A custom algorithm directly converted this voxel-based image into an OpenFOAM compatible mesh.

### 4.2 Material properties and model setup

The solid background was taken as calcite with density  $2710 \text{ kgm}^{-3}$ , Young’s modulus  $84.3 \text{ GPa}$  and Poisson’s ratio as 0.317. Pores were represented as void inclusions by removing corresponding mesh elements, ensuring zero stiffness and no load transfer within the pore space. The maximum pore size was  $20 \mu\text{m}$ , and the cubic computational domain measured  $500 \mu\text{m}$  per side, discretized with  $1.43 \mu\text{m}$  voxels. To minimize boundary artifacts, a  $50 \mu\text{m}$  pore-free margin was retained around all edges.

## 4.3 Boundary and loading conditions

Boundary conditions were defined using OpenFOAM's fixedDisplacementZeroShear formulation, corresponding to an ideal uniaxial compression test:

- One face along  $x$ -direction was fixed in the normal direction but allowed free tangential motion. The  $x$ -position of this face was zero.
- The opposite face was subjected to a uniform prescribed pressure of 10000 Pa.
- The remaining four faces were traction-free, allowing free lateral expansion.

This configuration yields a nearly homogeneous stress field in the solid matrix and ensures that pore induced perturbations remain isolated, consistent with the non-interacting inclusion assumption of DEM theory.

## 4.4 Solver Configuration

The main solver parameters were specified through the standard OpenFOAM dictionaries:

- system/controlDict – runtime control and data output
- system/fvSchemes – gradient and Laplacian discretization schemes,
- system/fvSolution – solver tolerance and algorithms
- constant/rheologyProperties – defines the isotropic elastic constants
- 0/U – boundary displacement and constraints
- system/decomposeParDict – domain decomposition for parallel execution

Each case was decomposed using “scotch” and run on MPI processes for parallel execution.

## 4.5 Execution of Simulation

Once the case and the solver setting is properly set, the simulation can be started by running series of commands from case directory as listed in Code Listing 1. This also generates a log file for each command. An example for generated log for “elasticSolidFoam” is shown in Code Listing 2.

```
checkMesh |& tee -a checkMesh.log
decomposePar |& tee -a decomposePar.log
mpirun -np {NP} {SOLVER} -parallel |& tee -a {SOLVER}.log
reconstructPar -latestTime |& tee -a reconstructPar.log
foamCalc components U -latestTime
patchAverage Ux Inlet -latestTime |& tee -a averageUxInlet.log
patchAverage Ux Outlet -latestTime |& tee -a averageUxOutlet.log
patchAverage Uy North -latestTime |& tee -a averageUyNorth.log
patchAverage Uy South -latestTime |& tee -a averageUySouth.log
  patchAverage Uz Top -latestTime |& tee -a averageUzTop.log
patchAverage Uz Bottom -latestTime |& tee -a averageUzBottom.log
foamToVTK -latestTime -fields '(U V epsilon sigma epsilonEq sigmaEq)'
```

*Code Listing 1: Commands for executing the openFOAM case. It generates a log file for each command executed.*

```

/*-----*/
|=====|
| \ \ / F ield | foam-extend: Open Source CFD
| \ \ / O peration | Version: 4.1
| \ \ / A nd | Web: http://www.foam-extend.org
| \ \ / M anipulation | For copyright notice see file Copyright
|-----*/

Build : 4.1-5832cfe256a5
Exec : elasticSolidFoam -parallel
Date : Sep 23 2025
Time : 13:58:29
Host : "DESKTOP-I391F98"
PID : 3238
CtrlDict :
"/mnt/d/Sanjay/OpenFOAM/EshelbyShapes/Rocks/GradualConcavity/cases/Ellipsoid_0.25_10K_0.0100_BLC/system/controlDict"
Case :
"/mnt/d/Sanjay/OpenFOAM/EshelbyShapes/Rocks/GradualConcavity/cases/Ellipsoid_0.25_10K_0.0100_BLC"
nProcs : 10
Slaves :
9
(
"DESKTOP-I391F98.3239"
"DESKTOP-I391F98.3240"
"DESKTOP-I391F98.3241"
"DESKTOP-I391F98.3242"
"DESKTOP-I391F98.3243"
"DESKTOP-I391F98.3244"
"DESKTOP-I391F98.3245"
"DESKTOP-I391F98.3246"
"DESKTOP-I391F98.3249"
)
.
.
.
Starting time loop

Time = 1

Predicting U, gradU and snGradU based on V,gradV and snGradV

DICPCG: Solving for Ux, Initial residual = 1, Final residual = 0.0997051, No Iterations 310
PCG: Solving for Uy, Initial residual = 0, Final residual = 0, No Iterations 0
PCG: Solving for Uz, Initial residual = 0, Final residual = 0, No Iterations 0
Time 1, Corrector 0, Solving for U using fvMatrix<Type>::solve, res = 1, rel res = 0.999979,
aitken = 0.1, inner iters = 0
DICPCG: Solving for Ux, Initial residual = 0.00133798, Final residual = 0.000133303, No Iterations
272
DICPCG: Solving for Uy, Initial residual = 1, Final residual = 0.0995175, No Iterations 168
DICPCG: Solving for Uz, Initial residual = 1, Final residual = 0.0976246, No Iterations 168
.
.
.
DICPCG: Solving for Uy, Initial residual = 1.00701e-06, Final residual = 7.95721e-07, No Iterations 1
DICPCG: Solving for Uz, Initial residual = 1.00389e-06, Final residual = 7.96211e-07, No Iterations 1
PCG: Solving for Ux, Initial residual = 7.8447e-07, Final residual = 7.8447e-07, No Iterations 0
PCG: Solving for Uy, Initial residual = 9.95113e-07, Final residual = 9.95113e-07, No Iterations 0
PCG: Solving for Uz, Initial residual = 9.9307e-07, Final residual = 9.9307e-07, No Iterations 0

Time 1, Solving for U, Initial residual = 1, Final residual = 9.95113e-07, Relative residual = 0, No
outer iterations 221
ExecutionTime = 86157.8 s ClockTime = 86835 s
Max epsilonEq = 3.79418e-07
Max sigmaEq = 36424.3
Found patch Outlet, writing y force and displacement to file
ExecutionTime = 86229.6 s ClockTime = 86909 s

End

Finalising parallel run

```



*Code Listing 2: Example log for elasticSolidFoam run in parallel using 10 threads.*

## 4.6 Post-Processing and effective modulus estimation

After convergence, displacement and stress fields were extracted at the outer boundaries. Average displacements were computed using the patchAverage utility for each pair of opposite faces. The difference between opposing face averages gives macroscopic strain, while the reaction forces yield macroscopic stress.

From these averages, Young's modulus was computed as the ratio of displacement difference to sample length ( $L$ ):

$$E = \frac{U_x^{Outlet} - U_x^{Inlet}}{L_x}$$
$$\nu_y = \frac{U_y^{North} - U_y^{South}}{U_x^{Inlet} - U_x^{Outlet}}, \quad \nu_z = \frac{U_z^{Top} - U_z^{Bottom}}{U_x^{Inlet} - U_x^{Outlet}}$$

The corresponding average normal stress were obtained from the reaction forces divided by the loaded surface area.

Using these quantities, the directional bulk and shear moduli were computed as:

$$K_i = \frac{E_i}{3(1 - 2\nu_i)}, \quad G_i = \frac{E_i}{2(1 + \nu_i)} \quad i = y, z$$

The approach provides a directional check on isotropy – if the pore distribution and boundary conditions are balanced,  $K_y \approx K_z$  and  $G_y \approx G_z$  within numerical tolerance.

## 5. Extended Effective Medium Theory

The Extended Differential Effective Medium (Ex-DEM) framework build upon the classical DEM theory (Norris, 1985) by introducing two perturbation coefficients,  $a$  and  $b$ , that account for the mechanical influence of non-ellipsoidal pore geometries.

In the classical DEM formulation, pores are idealized as ellipsoidal inclusions whose strain field is homogeneous and governed by Wu's tensor. Real rocks, however, contain pores with irregular, concave, and interconnected morphologies that produce non-uniform local stresses and departures from this assumption. The coefficients  $a$  and  $b$  therefore serve as geometric correction factors that scale the volumetric and shear components of the Eshelby-type inclusion response.

### 5.1 Formulation

The DEM differential equations for the evolution of bulk and shear moduli with porosity  $\phi$  are written as:

$$\frac{dK}{d\phi} = (K_i - K)P^*, \quad \frac{d\mu}{d\phi} = (\mu_i - \mu)Q^*$$

where,  $K$  and  $\mu$  are the effective moduli of the composite at porosity  $\phi$ ,  $K_i$  and  $\mu_i$  are the inclusion (pore) moduli (zero for voids), and  $P^*$  and  $Q^*$  are the pore compressibility and shear compliance factors, respectively, derived from Wu's tensor for an ellipsoidal inclusion.

The Extended DEM introduces two perturbation coefficients  $a$  and  $b$  that modify these geometric factors to account for complex pore shapes:

$$\frac{dK}{d\phi} = (K_i - K)aP^*, \quad \frac{d\mu}{d\phi} = (G_i - G)bQ^*$$

For an ideal ellipsoidal pore,  $a = b = 1$ , reducing the system to the classical DEM.

Departure of these coefficients from unity is typically associated with concave or irregular pores that enhance the shear compliance relative to volumetric compliance.

## 5.2 Numerical Fitting Procedure

The effective bulk and shear moduli obtained from the numerical simulations were used to determine the perturbation coefficients  $a$  and  $b$  of the Extended DEM model. For each pore geometry, the Ex-DEM equations were evaluated across a prescribed range of trial  $(a, b)$  values, while maintaining the same matrix stiffness and equivalent pore aspect ratios as in the corresponding simulations. The pore phase was modelled as a void inclusion, with both its bulk and shear moduli set to zero.

The optimal pair of coefficients  $(a, b)$  was identified by minimizing an objective function  $\Phi(a, b)$  based on the coefficient of determination ( $R^2$ ) between the simulated and model-predicted moduli:

$$\Phi(a, b) = |1 - R_K^2(a, b)| + |1 - R_\mu^2(a, b)|$$

where  $R_K^2$  and  $R_\mu^2$  denote the goodness of fit for the bulk and shear moduli, respectively, evaluated over all simulated porosity levels.

The resulting values of  $a$  and  $b$  directly quantify the geometric deviation of each pore family from the ideal ellipsoidal inclusion assumed in the classical DEM theory, thereby linking pore convexity and aspect ratio to the macroscopic elastic response.

## 6. Results

Numerical simulations were performed on synthetic digital rocks containing isolated, non-interacting pores of prescribed geometry and aspect ratio. These controlled conditions emulate the assumption of effective medium theories at dilute porosity, allowing a systematic assessment of how pore geometry influences the perturbation coefficients  $a$  and  $b$  in the extended DEM framework.

Table 1: Summary of equivalent pore aspect ratio and extended DEM coefficients ( $a$ ,  $b$ ) for different pore geometries.

Name	Original $\alpha$	$\delta$	$\chi$ (°)	Convexity	Equivalent $\alpha$	$a$	$b$	R2K	R2G
Ellipsoid	0.25	1.8	-	0.771	[1.0, 0.96, 1.00]	2.60	1.86	0.98	0.99
Ellipsoid	0.25	1.4	-	0.814	[1.0, 0.77, 1.00]	2.34	1.74	0.99	1.00
Ellipsoid	0.25	1.0	-	0.850	[1.0, 0.58, 1.00]	2.03	1.58	1.00	1.00
Ellipsoid	0.25	0.6	-	0.900	[1.0, 0.37, 0.96]	1.60	1.36	1.00	1.00
Ellipsoid	0.25	0.2	-	0.937	[1.0, 0.22, 0.89]	1.09	1.08	0.99	1.00
RhombohedralPore	-	-	60	0.794	[1.0, 0.47, 0.57]	1.86	1.55	1.00	1.00
RhombohedralPore	-	-	70	0.819	[1.0, 0.66, 0.75]	1.59	1.39	1.00	1.00
RhombohedralPore	-	-	80	0.839	[1.0, 0.79, 0.84]	1.41	1.28	1.00	1.00
RhombohedralPore	-	-	90	0.875	[1.0, 0.96, 0.96]	1.35	1.24	1.00	1.00

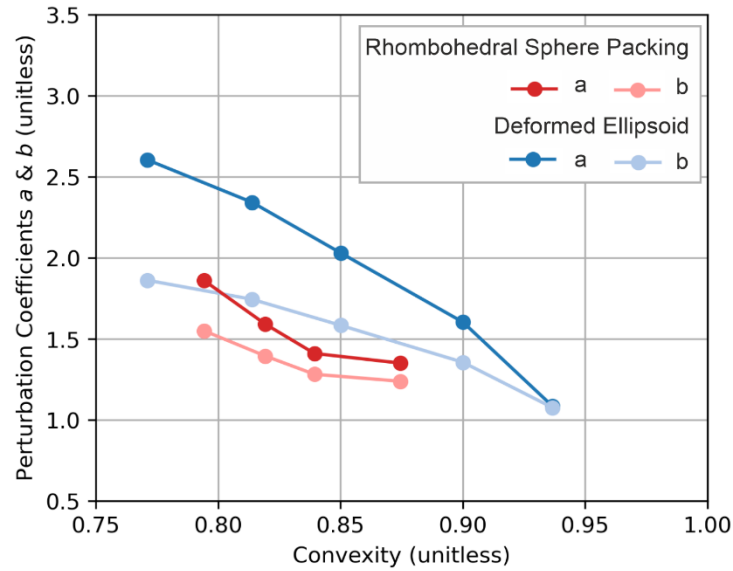


Figure 3: Variation of geometric perturbation coefficients  $a$  and  $b$  with pore geometry for deformed ellipsoids and rhombohedral sphere-packing configurations. Both coefficients increase with decreasing convexity, indicating stronger departures from ellipsoidal assumption.

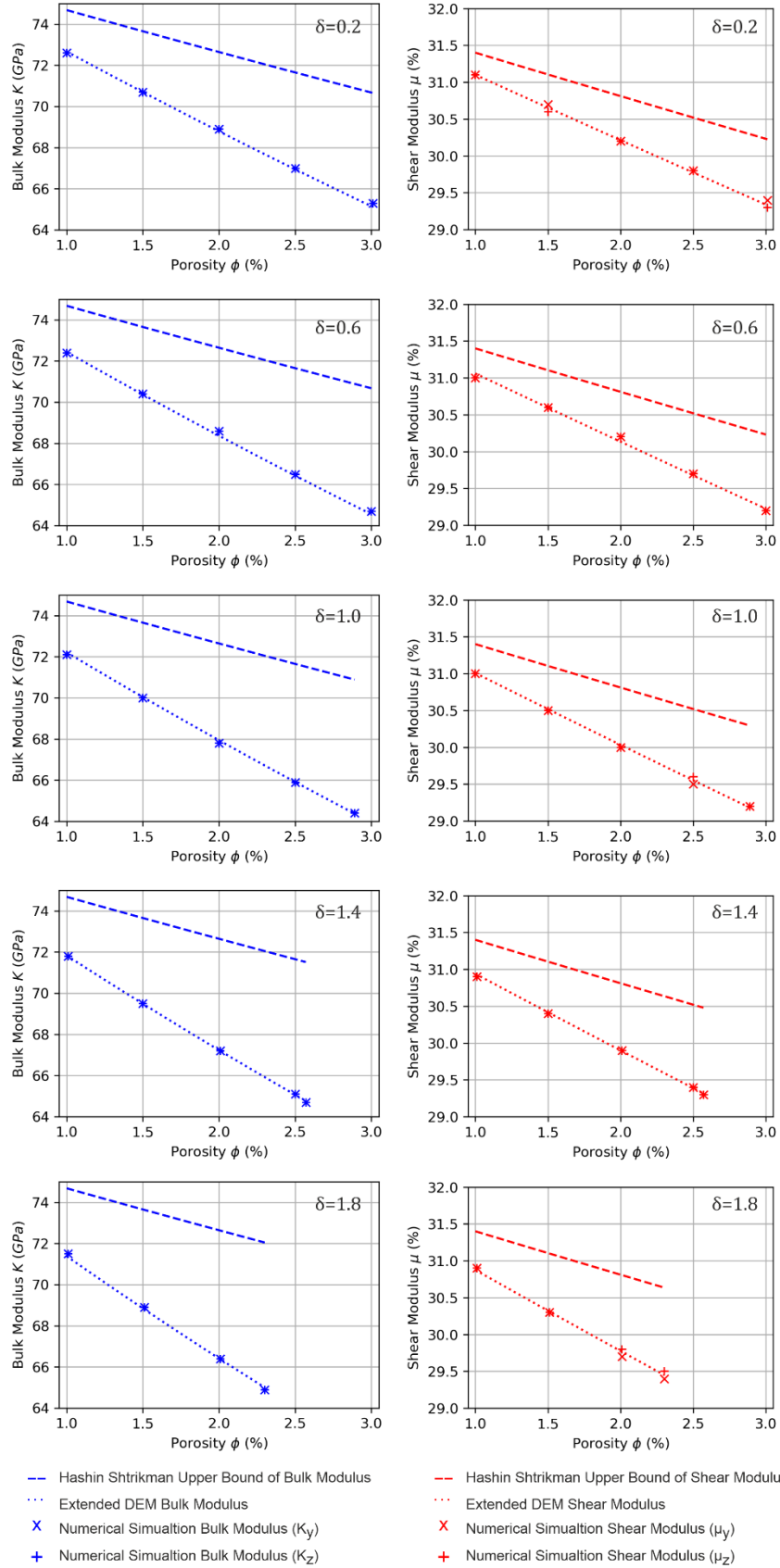
## 6.1 Ellipsoidal Pore Model with Gradually Varying Convexity

Table 1 summarizes the convexity controlling parameter  $\delta$ , convexity and the corresponding equivalent ellipsoid and extended DEM perturbation coefficients. The

corresponding fit quality i.e. determination of coefficient  $R^2$  for bulk and shear modulus is also listed in Table 1 and the corresponding fit can also be seen in Figure 4.

It can be observed that for increasing convexity the corresponding perturbation coefficients  $a$  and  $b$  increases monotonically (Figure 3).

Deformed Ellipsoidal Pore System



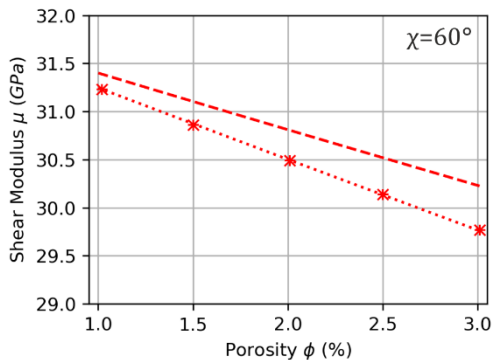
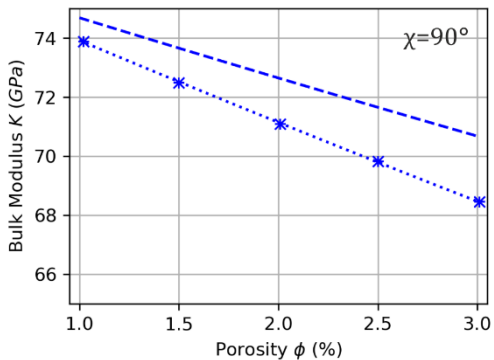
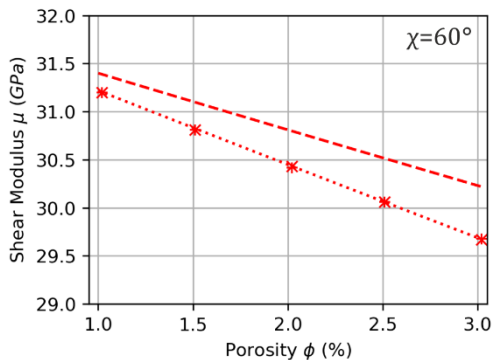
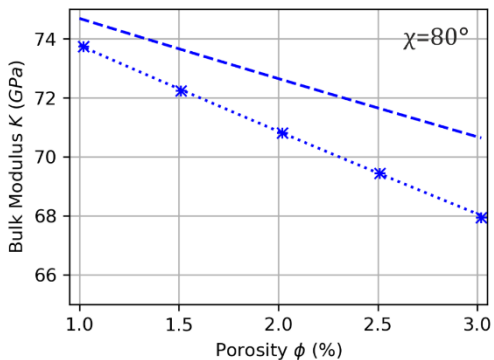
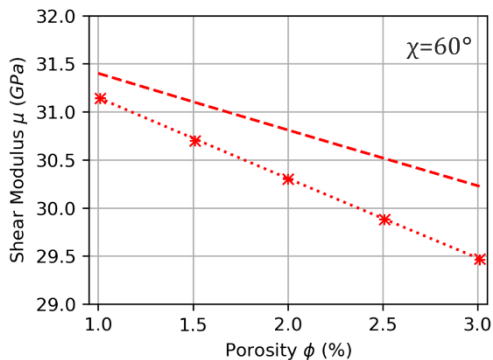
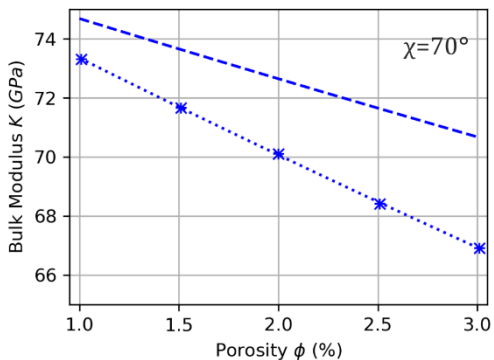
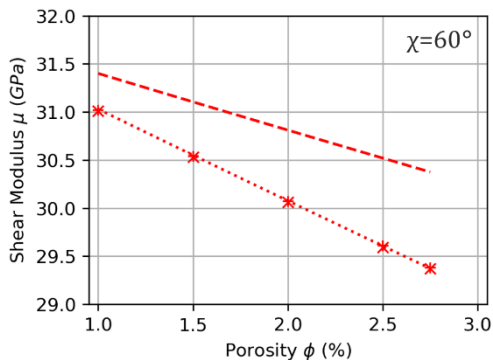
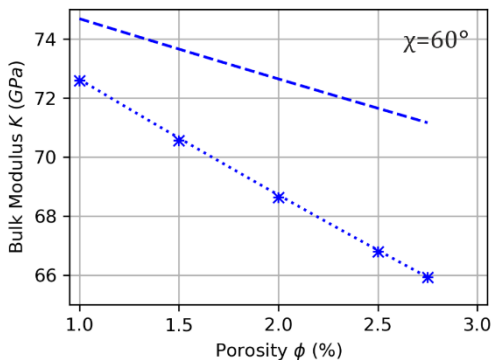
*Figure 4: Variation of the bulk and shear moduli with porosity for different values of the shape-controlling parameter  $\delta$ . As  $\delta$  increases, the slopes for both the bulk and shear modulus curves become steeper, indicating that the moduli decreases more rapidly with porosity for higher  $\delta$ . The Extended DEM predictions (dotted lines) accurately reproduce the simulated trends for both bulk and shear moduli, with coefficients of determination ( $R^2$ ) close to 1.0, demonstrating an excellent fit.*

## 6.2 Rhombohedral Sphere Packing

Table 1 summarizes the convexity controlling parameter  $\chi$ , convexity and the corresponding equivalent ellipsoid and extended DEM perturbation coefficients. The corresponding fit quality i.e. determination of coefficient  $R^2$  for bulk and shear modulus is also listed in Table 1 and the corresponding fit can also be seen in Figure 5.

It can be observed that for increasing convexity the corresponding perturbation coefficients  $a$  and  $b$  increases monotonically (Figure 3).

### Rhombohedral Pore System



- |     |  |     |  |
|-----|--|-----|--|
| --- | Hashin Shtrikman Upper Bound of Bulk Modulus | --- | Hashin Shtrikman Upper Bound of Shear Modulus  |
| ... | Extended DEM Bulk Modulus                    | ... | Extended DEM Shear Modulus                     |
| X   | Numerical Simualtion Bulk Modulus ( $K_Y$ )  | X   | Numerical Simualtion Shear Modulus ( $\mu_Y$ ) |
| +   | Numerical Simualtion Bulk Modulus ( $K_Z$ )  | +   | Numerical Simualtion Shear Modulus ( $\mu_Z$ ) |



*Figure 5: Variation of the bulk and shear moduli with porosity for different values of the shape-controlling parameter  $\chi$ . As  $\chi$  increases, the slopes for both the bulk and shear modulus curves becomes gentler, indicating that the moduli decrease less rapidly with porosity for higher  $\chi$ . The Extended DEM predictions (dotted lines) accurately reproduce the simulated trends for both bulk and shear moduli, with coefficients of determination ( $R^2$ ) close to 1.0, demonstrating an excellent fit.*

## 7. Data Availability

All the OpenFOAM case files, simulation results, mesh, stress and strain fields along with simulation log files are available for each case with links provided in record description.